Funding:

Seismic Hazard due to Fluid Injections.*

Cole Lord-May [a], Jordi Baró [a,b,c,*], David Eaton[b], Jörn Davidsen [a]

[a] *Complexity Science Group, Dept. of Physics and Astronomy, U. of Calgary, Calgary, AB, T2N 1N4, Canada.*
[b] *Dept. of Geosciences, U. of Calgary, Calgary, AB, T2N 1N4, Canada.*
[c] *Centre for Mathematical Research (CRM), Barcelona, 08193, Spain.*

* jbaro@crm.cat

*work under revision, submitted to *Physical Review Letters*.
Display presented at session **SM3.2** of the **#shareEGU20** online meeting.

Open chatroom with the authors on **Monday, 04 May 2020, 10:45-12:30 CET** at:

https://meetingorganizer.copernicus.org/EGU2020/EGU2020-6334.html

Comments are welcomed befor 30 May 2020.

Author notes:

This display format is rather new. We need to improvise in the format and contemplate possible contingencies. This is the adaptation of a poster, intended to optimize the opportunities offered by the new display format: halfway between a poster and slide show. Find the original poster at the end of the document.

Officially, the chatroom will be open on **Monday, 04 May 2020, 10:45-12:30 CET** at the following link:

https://meetingorganizer.copernicus.org/EGU2020/EGU2020-6334.html

The presenting author will also be available from **14:00-15:45 CET** on the same day **4 May 2020**, at chatroom:

https://meetingorganizer.copernicus.org/EGU2020/EGU2020-4948.html

Please, feel free to leave comments at any other time **before 30 May 2020**, at the same links.

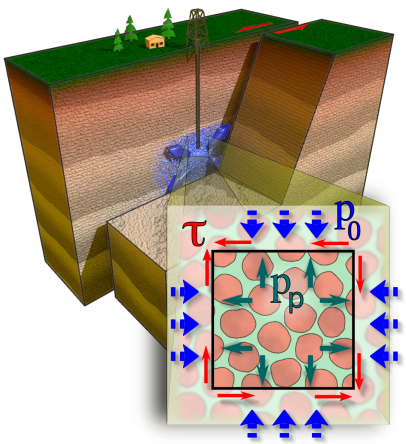

Natural and anthropogenic processes involving the **injection** or **migration of fluids** within rock formations can **induce earthquakes**. Field observations led to the formulation of **three different paradigms** relating seismic hazards and injected volume (V) [*1*], useful to develop risk mitigation strategies [*2*]. According to them fluid-induced earthquakes are either:

A) small and their number is proportional to V [*3,4*];

B) bounded in size and magnitude by the stimulated area [*5*];

C) indistinguishable from tectonic earthquakes [*6*].

All three paradigms naturally coexist in the **unified conceptual model** presented here, accounting for **stick-slip mechanics** [*7*] and **non-homogeneous pore-pressure stimulation** [*8*] caused by fluid injection in a prestressed region. The loading history and heterogeneity of the host medium determine which of the three paradigms dominates. In **non-tectonic settings two populations** of events triggered at different pore-pressure levels with different Gutenberg-Richter b-values are superposed. Stress-levels and V determine their proportions. In active **tectonic settings**, fluid injection triggers **tectonic earthquakes**.

We consider a 2D-lattice of sites (l) with local **pore pressure** ($p_{p,l}$), scalar **stress** field ($\tau_{s,l}$), and **strength** thresholds (s_l).

1) Fluid flows through channels connecting adjacent sites (i, j) with random permeability $\nu_{i,j}$.

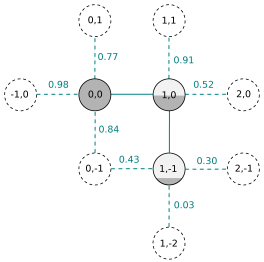

We consider a 2D-lattice of sites (l) with local **pore pressure** ($p_{p,l}$), scalar **stress** field ($\tau_{s,l}$), and **strength** thresholds (s_l).

1) Fluid flows through channels connecting adjacent sites (i, j) with random permeability $\nu_{i,j}$.

The fluid front advances through the connection at front $i \to j$ with higher $p_{p,i} - p_{p,j} + \nu_{ij}$.

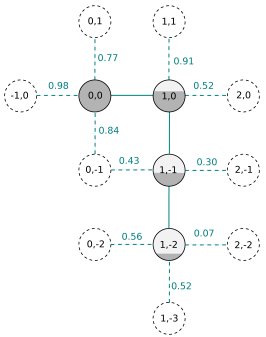

We consider a 2D-lattice of sites (l) with local **pore pressure** ($p_{p,l}$), scalar **stress** field ($\tau_{s,l}$), and **strength** thresholds (s_l).

1) Fluid flows through channels connecting adjacent sites (i, j) with random permeability $\nu_{i,j}$.

The fluid front advances through the connection at front $i \to j$ with higher $p_{p,i} - p_{p,j} + \nu_{ij}$.

2) The pressure profiles ($p_p(d)$) decay exponentially with distance (d) from source. A minimum pressure gradient $p_{\min}$ is imposed at max. distance from source.

Tuning $p_{\min}$ we control a transition form an **invasion percolation** limit [8] (capillarity and/or brittle poromechanics dominate) to a **viscous flow** limit.

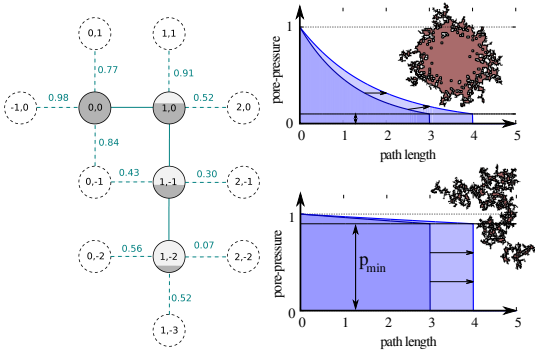

We consider a 2D-lattice of sites (l) with local **pore pressure** ($p_{p,l}$), scalar **stress** field ($\tau_{s,l}$), and **strength** thresholds (s_l).

1) Fluid flows through channels connecting adjacent sites (i, j) with random permeability $\nu_{i,j}$.

The fluid front advances through the connection at front $i \to j$ with higher $p_{p,i} - p_{p,j} + \nu_{ij}$.

2) The pressure profiles ($p_p(d)$) decay exponentially with distance (d) from source. A minimum pressure gradient $p_{\min}$ is imposed at max. distance from source.

Tuning $p_{\min}$ we control a transition form an **invasion percolation** limit [8] (capillarity and/or brittle poromechanics dominate) to a **viscous flow** limit.

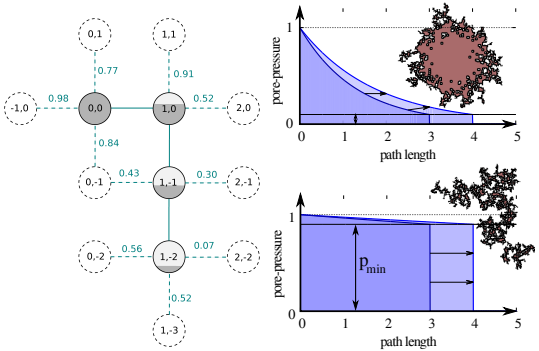

3) Fractures are generated following a simplified Mohr-Coulomb condition:

$$\tau_l > \tau_{s,l} = \tau_{c,l} + \mu_l(p_{0,l} - p_{p,l}) = s_l - p_p$$

Strengths are uniformly sampled $s_l \sim \mathcal{U}(s_{\min}, s_{\max})$.
We consider spring-block model interactions [7]:
On slip $\tau_l \to 0$ and $\delta\tau_l = \alpha\tau_l$ to n.n..

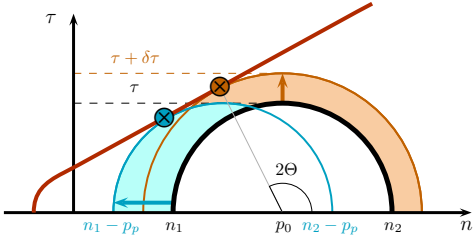

We consider a 2D-lattice of sites (l) with local **pore pressure** ($p_{p,l}$), scalar **stress** field ($\tau_{s,l}$), and **strength** thresholds (s_l).

1) Fluid flows through channels connecting adjacent sites (i, j) with random permeability $\nu_{i,j}$.

The fluid front advances through the connection at front $i \to j$ with higher $p_{p,i} - p_{p,j} + \nu_{ij}$.

2) The pressure profiles ($p_p(d)$) decay exponentially with distance (d) from source. A minimum pressure gradient $p_{\min}$ is imposed at max. distance from source.

Tuning $p_{\min}$ we control a transition form an **invasion percolation** limit [8] (capillarity and/or brittle poromechanics dominate) to a **viscous flow** limit.

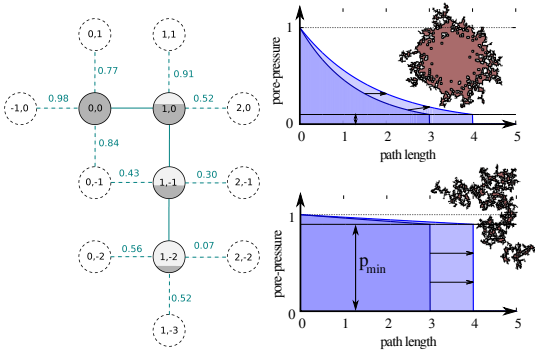

3) Fractures are generated following a simplified Mohr-Coulomb condition:

$$\tau_l > \tau_{s,l} = \tau_{c,l} + \mu_l(p_{0,l} - p_{p,l}) = s_l - p_p$$

Strengths are uniformly sampled $s_l \sim \mathcal{U}(s_{\min}, s_{\max})$.
We consider spring-block model interactions [7]:
On slip $\tau_l \to 0$ and $\delta\tau_l = \alpha\tau_l$ to n.n..

Fractures initiate through (wet) slip by increase in $p_{p,l}(t)$

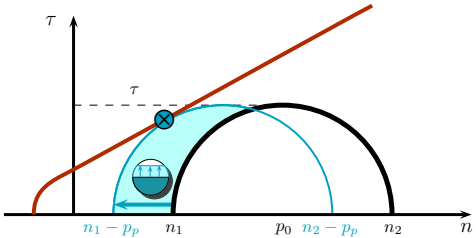

We consider a 2D-lattice of sites (l) with local **pore pressure** ($p_{p,l}$), scalar **stress** field ($\tau_{s,l}$), and **strength** thresholds (s_l).

1) Fluid flows through channels connecting adjacent sites (i, j) with random permeability $\nu_{i,j}$.

The fluid front advances through the connection at front $i \to j$ with higher $p_{p,i} - p_{p,j} + \nu_{ij}$.

2) The pressure profiles ($p_p(d)$) decay exponentially with distance (d) from source. A minimum pressure gradient $p_{\min}$ is imposed at max. distance from source.

Tuning $p_{\min}$ we control a transition form an **invasion percolation** limit [8] (capillarity and/or brittle poromechanics dominate) to a **viscous flow** limit.

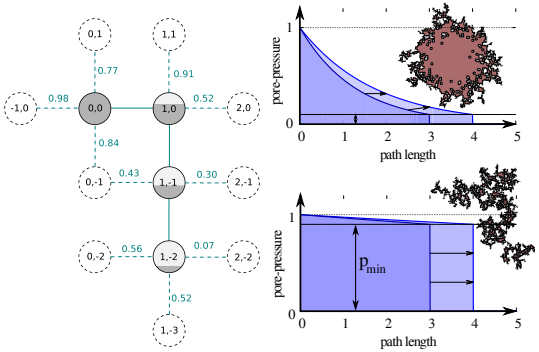

3) Fractures are generated following a simplified Mohr-Coulomb condition:

$$\tau_l > \tau_{s,l} = \tau_{c,l} + \mu_l(p_{0,l} - p_{p,l}) = s_l - p_p$$

Strengths are uniformly sampled $s_l \sim \mathcal{U}(s_{\min}, s_{\max})$.
We consider spring-block model interactions [7]:
On slip $\tau_l \to 0$ and $\delta\tau_l = \alpha\tau_l$ to n.n..

Fractures initiate through (wet) slip by increase in $p_{p,l}(t)$

and propagate through (dry) slip due to $\delta\tau_l$.

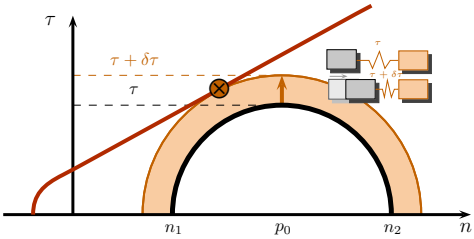

All events are initiated at site l by variations of the local pore pressure ($p_{p,l}(t)$). These can be either caused by:

(i) the propagation of fluid to newly percolated regions. This initiates events at the **boundary** through the exploration of new accessible areas (see [*8*]) and exhibit spatial clustering; or

(ii) Global changes in the $p_p(d)$ profile when the max. path length is increased. This initiates events in the whole **area** through the simultaneous activation of multiple sites and exhibit temporal clustering *.

Overall, we observe a migration of event-locations with $V^{0.5}$.

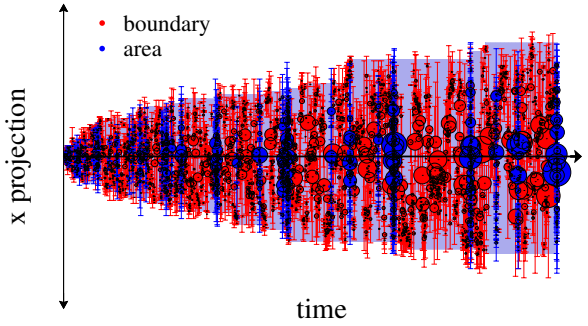

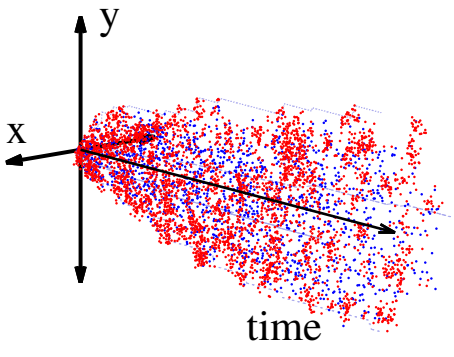

* These features are mere artifacts of the pore-pressure profile as implemented in our model.

We consider three different (related) event magnitudes:

- A: The **area** of fracture or number of sites slipped at least once in the event;
- S: The **size** or total number of slips;
- $\Delta := \sum_{i \in \{\text{slips}\}} \tau_{\text{s},i}$: The **total stress** released.

We assume proportionality between Δ and the moment released ($\mathcal{M}_0$).

We observe:

- A scaling relation with a transition due to finite size effects: $A \approx S(\sim \Delta) \ \rightarrow \ A \propto S^{2/3}$.
- A power-law distribution of Δ (with exponent $\gamma_\Delta := 3/2b_\Delta + 1$).
- High variability in power-law exponents or b-values (as shown in [*4*]):
  - **high b-values** ($\gamma_{\Delta,\text{I}} \approx 2.6$) for **low stress levels** (high $s_{\max}$).
  - **low b-values** ($\gamma_{\Delta,\text{II}} \approx 1.27$) for **high stress levels** (low $s_{\max}$).
- We argue that this transition is caused by the co-existence of **critical** and **subcritical** events.
  (see next)

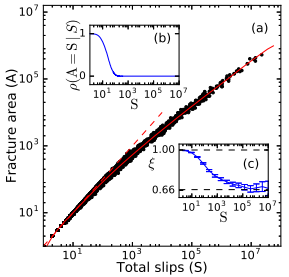

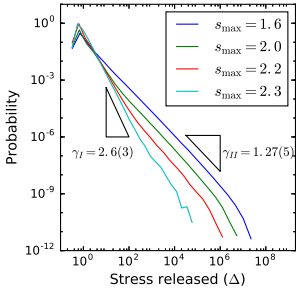

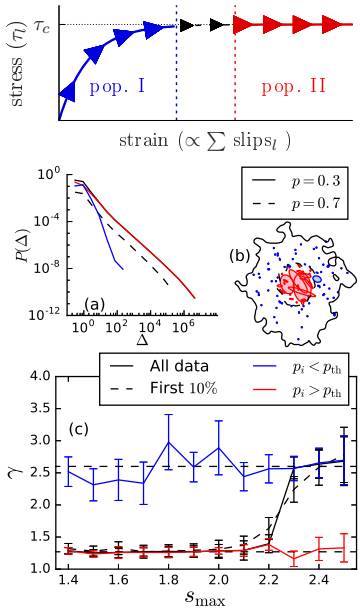

The toy model predicts **three** different kinds of events:

1) In **non-tectonic** settings, two populations coexist, depending on the injected volume (V) and the stress level ($s_{\rm max}$):

$$dN(\mathcal{M}_0) \propto (\boldsymbol{x}_{\rm I}(s_{\rm max})\boldsymbol{P}_{\rm I}(\mathcal{M}_0; s_{\rm max}) + \boldsymbol{x}_{\rm II}(s_{\rm max})\boldsymbol{P}_{\rm II}(\mathcal{M}_0; s_{\rm max}))\, dV$$

Population I: A stationary front of **subcritical** regions where ($p_p < p_c$); Superposition of power-law distributions with different cutoffs $\Rightarrow$ steep power-law ($\gamma_{\Delta,\rm I} = \frac{3}{2} b_{\Delta,\rm I} + 1 \approx 2.6$) of small events [**3**,**4**]:

$$\boldsymbol{P}_{\rm I}(\mathcal{M}_0; \gamma_{\rm I}, \mathcal{M}_{0,c}) d\mathcal{M}_0 = \left(\frac{\mathcal{M}_0}{\mathcal{M}_{0,c}}\right)^{-\gamma_{\rm I}} \frac{\gamma_{\rm I} - 1}{\mathcal{M}_{0,c}} d\mathcal{M}_0$$

Population II: **Critical** regions close to injection ($p_p \gtrsim p_c$) bounded by fluid [**5**]; critical distribution of spring-blocks in 2D; ($\gamma_{\Delta,\rm II} \approx 1.27$):

$$\boldsymbol{P}_{\rm II}(\mathcal{M}_0; \gamma_{\rm II}, \mathcal{M}_{0,s}, M_{0,c}) d\mathcal{M}_0 = \frac{\mathcal{M}_0^{-\gamma_{\rm II}} \exp(-\mathcal{M}_0/\mathcal{M}_{0,s})}{\Delta_c^{1-\gamma_{\rm II}} \Gamma\left(1-\gamma_{\rm II}, \frac{\mathcal{M}_{0,c}}{\mathcal{M}_{0,s}}\right)} d\mathcal{M}_0$$

where: $\log_{10}(\mathcal{M}_{0,s}) = \Lambda(s_{\rm max}) + \eta(s_{\rm max}) \log_{10}(V)$

Hence, the characteristic sizes of pop. II increase with V.

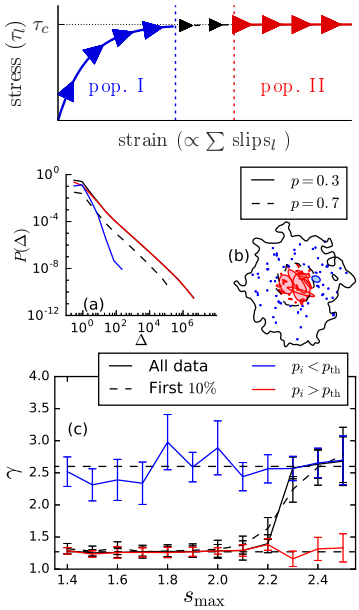

The toy model predicts **three** different kinds of events:

2) In a (SOC) critically loaded **tectonic** setting, events are triggered by p_p but unbounded in space [*6*].
All events belong to a single category:

Population III: **Critical** distribution of spring-block in 2D; ($\gamma_{\Delta,\rm II} \approx 1.27$):

$$dN(\mathcal{M}_0) \propto \boldsymbol{P}_{\rm III}(\mathcal{M}_0; s_{\rm max}) dV \; ; \quad \boxed{\boldsymbol{P}_{\rm III}(\mathcal{M}_0) d\mathcal{M}_0 = \left(\frac{\mathcal{M}_0}{\mathcal{M}_{0,c}}\right)^{-\gamma_{\rm II}} \frac{\gamma_{\rm II} - 1}{\mathcal{M}_{0,c}} d\mathcal{M}_0}$$

*Notice that **pop. III** would appear as a natural extension of **pop. II** to criticality when considering a good proxy for the stress-levels. In our case, tuning $s_{\rm max}$ is not enough to bring the reservoir to critical stress levels. We use alternative simulation with critically pre-stressed reservoirs instead.

Although the **micromechanical model** represents an oversimplified picture of the phenomena, the equivalent **statistical model** is based upon reasonable assumptions, provides some new insights on the expected hazard measurements, and is able to reconcile the three different paradigms [*1*]:

Hazard Measurement 1:
Examples of $\mathcal{M}_0 \sim \Delta$. By fitting $\{\hat{x}_{II},\ \hat{\Lambda},\ \hat{\eta}\}$. Cumulative number larger than Δ (as reported in [*4,5*]):

$s_{\max} = 2.2$ $\qquad$ $s_{\max} = 1.8$

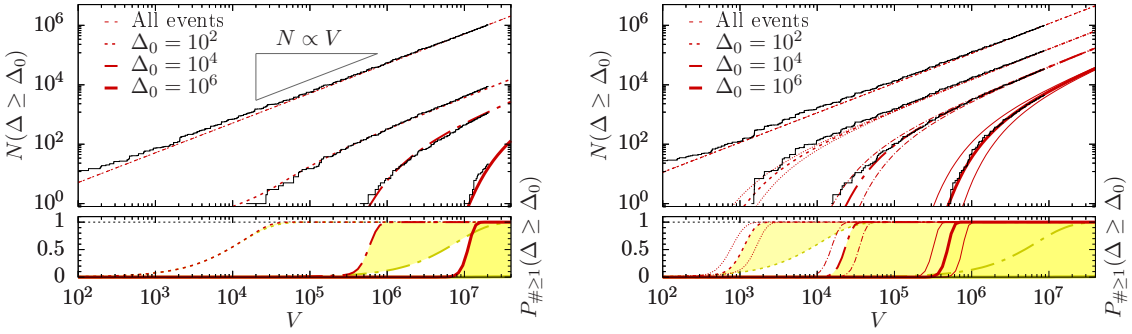

Lower panels show the inverse of the survival rate, i.e. the probability for the first record event above Δ_0. Yellow lines represent the prediction considering only **pop. I**.

Although the **micromechanical model** represents an oversimplified picture of the phenomena, the equivalent **statistical model** is based upon reasonable assumptions, provides some new insights on the expected hazard measurements, and is able to reconcile the three different paradigms [*1*]:

Hazard Measurement 2:
Record seismic moment, i.e. seismic moment of the stronger event up to the injection of V (as reported in [*1*]):

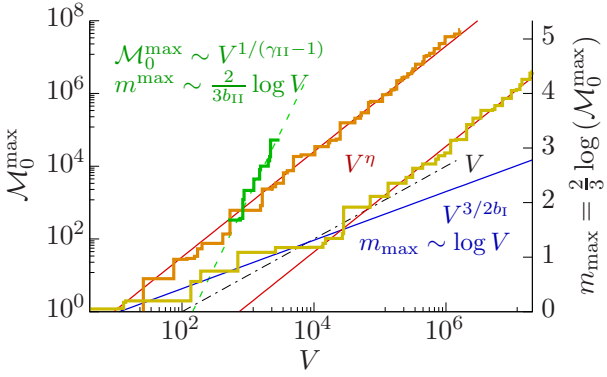

proportionality: $\mathcal{M}_0^{\max} \sim V$ (exponents in [*9*]).

pop. I dominates (small events, model **A** [*3*,*4*]).

pop. II dominates (bounded events, model **B** [*5*]).

Orange line: Numerical results for **high** stress level ($s_{\max} = 1.4$), always pop. II.

Yellow line: Numerical results for **low** stress level ($s_{\max} = 2.2$), **pop. I** $\rightarrow$ **pop. II**.

Tectonic setting (**pop III**) (model **C** [*6*]).

[1] D. W. Eaton, N. Igonin (2020) *The Leading Edge* **37**:2, 135-140 *10.1190/tle37020135.1*

[2] T. Ader, et al. (2019), *J. Seismol*. *10.1007/s10950-019-09853-y*

[3] A. McGarr (1976), *J. of Geophs. Res.* **81**, 1487 *10.1029/JB081i008p01487*

[4] C. Dinske, S. Shapiro (2013), *J. Seismol.* **17**: 13: *doi:10.1007/s10950-012-9292-9*

[5] S. Shapiro, O. Krüger C. Dinske, (2013) *J. of Geophs. Res. Solid Earth* **118**, 3557 *10.1002/jgrb.50264*

[6] N. van der Elst et al. (2016), *J. of Geophs. Res. Solid Earth* **121**, 4575 *10.1002/2016JB012818*

[7] Y. Ben-Zion, J. Rice (1993), *J. of Geophs. Res. Solid Earth* **98**, 14109 *10.1029/93JB01096*

[8] J. Norris, D. Turcotte, J. Rundle (2014), *Physical Review E* **89**, 022119 *10.1103/PhysRevE.89.022119*

[9] A. McGarr (2014), *J. of Geophs. Res. Solid Earth* **119**, 1008 *10.1002/2013JB010597*

[10] S. Shapiro, et al. (2011), *Geophysics* **76**:6, WC55-WC63 *10.1190/geo2010-0349.1*

[11] S. Shapiro, et al. (2010), *The Leading Edge* **29**:3, 304-309 *10.1190/1.3353727*

Supplementary Information

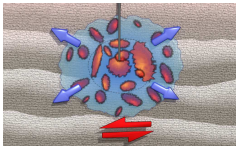

Unified model: The results obtained from the numerical simulations of the conceptual micromechanical model presented here can be described in terms of a unified statistical model. Given a subcritical distribution of strength values s_i, the general solution can be interpreted as a superposition of two populations of events (population I and II) such that the number of events: $dN(\mathcal{M}_0 > \mathcal{M}_0|t) = 10^{\Sigma} V(t) \left(x_{\mathrm{I}} P_{\mathrm{I}}(\mathcal{M}_0 > \mathcal{M}_0) + x_{\mathrm{II}} P_{\mathrm{II}}(\mathcal{M}_0 > \mathcal{M}_0|t)\right) dt$ where: $P_{\mathrm{I}}(\mathcal{M}_0 > \mathcal{M}_0) = \left(\mathcal{M}_0/\mathcal{M}_{0,c}\right)^{-\frac{2}{3}b_{\mathrm{I}}}$; $P_{\mathrm{II}}(\mathcal{M}_0 > \mathcal{M}_0|t) = \Gamma\left(-2b_{\mathrm{II}}/3, \mathcal{M}_0/\mathcal{M}_0^*(t)\right) / \Gamma\left(-2b_{\mathrm{II}}/3, \mathcal{M}_{0,c}/\mathcal{M}_0^*(t)\right)$, $\Gamma(b, x)$ is the upper incomplete Gamma function and Σ is an absolute seismogenic index. We assume M_0 to be proportional to S or Δ. Events in population I have intrinsic characteristic scales ($1 < 2b_{\mathrm{I}}/3$) and are nucleated at low pore-pressures (blue region out of the dashed line in the side diagram). The distribution of Population II is fat-tailed ($0 < 2b_{\mathrm{II}}/3 < 1$) but constrained inside a region delimited by a lower pore-pressure value (inside the dashed line) imposing a characteristic maximum scale $\mathcal{M}_0^*$. The unified model is able to reproduce the statistical properties of micro-seismic events predicted by the following three paradigms.

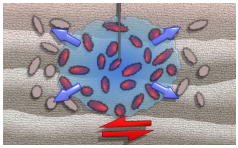

Paradigm A: Microseismic events are contained within the stimulated area and occur upon the activation (color patches) of inactive (grey patches) pre-existing fractures which partially determine a time-independent distribution of seismic moments [*4,10*]. The number of susceptible fractures and the probability of activation increases with pore-pressure [*4,10*]. Hence, the number of fractures above a seismic moment $\mathcal{M}_0$ reads $N(\mathcal{M}_0 > \mathcal{M}_0|t) = 10^{\Sigma} V(t) P(\mathcal{M}_0 > \mathcal{M}_0)$. The seismogenic index Σ completely determines the hazard rates and is observed to be constant over time in several HF and EGS opearations [*11*]. The maximum moment in a sequence of seismic events is determined by record statistics, and its expected value can be estimated by inverting $N(\mathcal{M}_0 > \mathcal{M}_0^{\max}|t) = 1$. Other models [*9*] impose constrains in energy, giving rise to time-dependencies in the absolute Σ and alternative $\mathcal{M}_0(V)$ relations.
In terms of the unified model: Fractures in paradigm A are statistically similar to population I, and compatible with our numerical results at low stress levels (high $s_{\max}$ values) and small injection volumes (yellow lines here). In that regime: $\mathcal{M}_0^{\max} \sim V^{\frac{3}{2b_{\mathrm{I}}}}$ (blue line here).

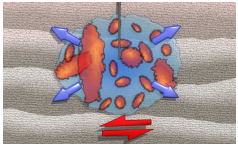

Paradigm B: Dynamic or pre-existing fractures have a typical GR distribution with fat tails, i.e. large events are statistically relevant. However, fractures are constrained in size to fit within the stimulated area (blue area in the left panel), i.e. there exists a maximum fracture area that increases over time in proportion to the total volume injected. The effective seismogenic index Σ is magnitude dependent and evolves in time in a non-scaling relation with $\mathcal{M}_0$. This can be interpreted as a lack of large earthquakes given Σ corrected at long times [**?**]. To be more precise, $P(\mathcal{M}_0 > \mathcal{M}_0|V(t)) \approx P(\mathcal{M}_0/\mathcal{M}_0^*(V(t)))$. This characteristic size $\mathcal{M}_0^*(V) \sim V^{\eta}$ dominates the record statistics. Hence, the expected maximum moment $\mathcal{M}_0^{\max} \sim V^{\eta}$ (red lines in here). Large microseismic events in HF and EGS operations are better described within this paradigm [*10*].
In terms of the unified model: Paradigm B is compatible with the statistics of population II, which dominate at long injection times, specially at high stress levels (low $s_{\max}$, e.g. orange line in here). The lack of large events at early times discussed by S. Shapiro et al. (2011) [*10*] is observed here.

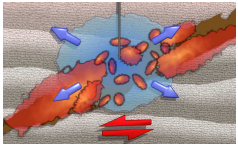

Paradigm C: Particularly strong events related with fluid injections can occur in the vicinity of critically loaded tectonic settings (represented in the left panel with a brown shadow). In such cases, earthquakes triggered by fluid injection are indistinguishable from tectonic earthquakes and can expand without any constrain imposed by the size of the stimulated area. The probability of event nucleation is still proportional to the injected volume, following the same arguments provided in [*4*]. Hence, the statistics are Gutenberg-Richter and determined by the tectonic setting [**?**]. Considering an unbounded power-law distribution of moments, the expected maximum moment is again determined by record statistics in a stationary distribution: $\mathcal{M}_0^{\max} \sim V^{\frac{3}{2b}}$, where b is the b-value of the tectonic setting (green dashed line here).
In terms of the unified model: Paradigm C is reproduced by partly or entirely pre-loading the reservoir to the critical point through shear-stress driving. The results are shown in the green solid line here.

Seismic Hazard due to Fluid Injections.

Cole Lord-May [a], Jordi Baró [a,b,c], David Eaton [b], Jörn Davidsen [a]

[a] Complexity Science Group, Dept. of Physics and Astronomy, Univ. of Calgary, Calgary, AB, T2N 1N4, Canada.
[b] Dept. of Geosciences, Univ. of Calgary, Calgary, AB, T2N 1N4, Canada.
[c] Centre for Mathematical Research (CRM), Barcelona, 08193, Spain.

NSERC CRSNG · Microseismic Industry Consortium · AXA Research Fund

Natural and anthropogenic processes involving the injection or migration of fluids within rock formations can induce earthquakes. Field observations led to the formulation of three different paradigms relating seismic hazards and injected volume (V) [*1*]. According to them fluid-induced earthquakes are either:

1) small and their number is proportional to V [*2,3*];

2) bounded by the affected area such that their size also scales with V [*4*];

3) indistinguishable from tectonic earthquakes [*5*].

All three paradigms naturally coexist in the present unified conceptual model accounting for stick-slip mechanics and non-homogeneous pore-pressure stimulation caused by fluid injection in a prestressed region. The loading history and heterogeneity of the host medium determine which of the three paradigms dominates. In non-tectonic settings two populations of events triggered at different pore-pressure levels with different Gutenberg-Richter b-values are superposed. Stress-levels and V determine their proportions. In active tectonic settings, fluid injection triggers tectonic earthquakes.

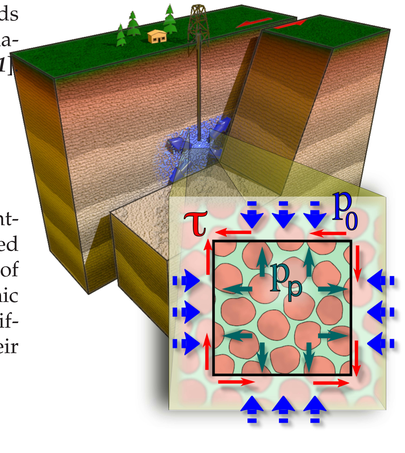

Events are initiated by $p_{p,l}(t)$ either by (i) propagation of fluid to new percolated regions (generates spatial clustering); or (ii) global changes in p_p (temporal clustering).

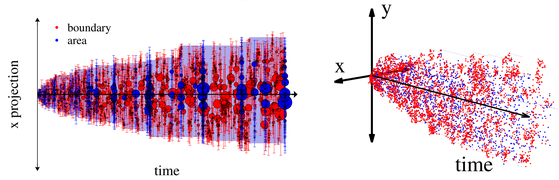

Three different (related) event magnitudes:

- A: Area of fracture or n. of sites slipped;
- S: Total n. slips or size;
- Stress released $\Delta := \sum_{i\in\{\text{slips}\}} \tau_{s,i}$. (assumed $\Delta \propto \mathcal{M}_0$)

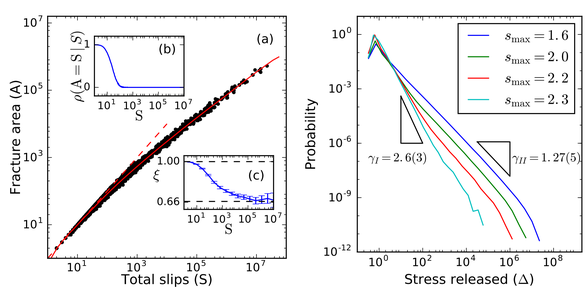

Transition by finite size effects: $A \approx S(\sim \Delta) \rightarrow A \propto S^{2/3}$. Power-law distribution of Δ (with exponent $\gamma_\Delta = b_\Delta + 1$). High variability (as rep. in [*3*]): high values ($\gamma_{\Delta,\mathrm{I}} \approx 2.6$) for low stress levels; low values ($\gamma_{\Delta,\mathrm{II}} \approx 1.27$) for high stress levels, due to the co-existence of critical and sub-critical events.

1) Fluid flow: 2D-lattice of sites with local p_p and links with random permeability ν. Fluid front advances through the connection at front $i \rightarrow j$ with higher $p_{p,i} - p_{p,j} + \nu_{ij}$. p_p decays exponentially with distance from source. A minimum pressure gradient $p_{\min}$ is imposed at max. distance from source: Transition form invasion percolation [*6*] (capillarity and/or brittle poromechanics) to viscous flow.

2) Fracture: Mohr-Coulomb condition at site l:

$$\tau_l > \tau_{s,l} = \tau_{c,l} + \mu_l(p_{0,l} - p_{p,l}) = s_l - p_p$$

Resilience $s_l \sim \mathcal{U}(s_{\min}, s_{\max})$. Spring-block model interactions [*7*]. On slip $\tau_l \rightarrow 0$ and $\delta\tau_l = \alpha\tau_l$ to n.n..

Fractures initiate through a (wet) slip due to changes in $p_p(t)$ and propagate through (dry) slip due to $\delta\tau_l$.

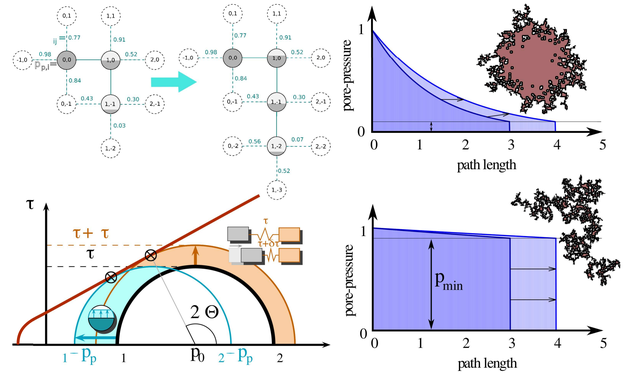

The toy model predicts **three** different kinds of events:

1) In **non-tectonic** settings, two populations coexist, depending on injected volume (V) and stress level ($s_{\max}$):

$$dN(\mathcal{M}_0) \propto (\boldsymbol{x}_{\mathrm{I}}(s_{\max})\boldsymbol{P}_{\mathrm{I}}(\mathcal{M}_0; s_{\max}) + \boldsymbol{x}_{\mathrm{II}}(s_{\max})\boldsymbol{P}_{\mathrm{II}}(\mathcal{M}_0; s_{\max}))\, dV$$

- **pop. I**: Stationary front of **subcritical** regions ($p_p < p_c$); Superposition of power-law distributions with different cutoffs $\Rightarrow$ steep power-law ($\gamma_{\Delta,\mathrm{I}} = \frac{3}{2}b_{\Delta,\mathrm{I}} + 1 \approx 2.6$) of small events [*2,3*]:

$$\boldsymbol{P}_{\mathrm{I}}(\mathcal{M}_0; \gamma_{\mathrm{I}}, \mathcal{M}_{0,c})d\mathcal{M}_0 = \left(\frac{\mathcal{M}_0}{\mathcal{M}_{0,c}}\right)^{-\gamma_{\mathrm{I}}} \frac{\gamma_{\mathrm{I}} - 1}{\mathcal{M}_{0,c}} d\mathcal{M}_0$$

- **pop. II**: **Critical** regions close to injection ($p_p \gtrsim p_c$) bounded by fluid [*4*]; critical distribution of spring-blocks in 2D; ($\gamma_{\Delta,\mathrm{II}} \approx 1.27$):

$$\boldsymbol{P}_{\mathrm{II}}(\mathcal{M}_0; \gamma_{\mathrm{II}}, \mathcal{M}_{0,s}, M_{0,c})d\mathcal{M}_0 = \frac{\mathcal{M}_0^{-\gamma_{\mathrm{II}}} \exp(-\mathcal{M}_0/\mathcal{M}_{0,s})}{\Delta_c^{1-\gamma_{\mathrm{II}}}\Gamma\left(1-\gamma_{\mathrm{II}}, \frac{\mathcal{M}_{0,c}}{\mathcal{M}_{0,s}}\right)} d\mathcal{M}_0$$

where: $\log_{10}(\mathcal{M}_{0,s}) = \boldsymbol{\Lambda}(s_{\max}) + \eta(s_{\max})\log_{10}(V)$

2) In a (SOC) critically loaded **tectonic** setting, events are triggered by p_p but unbounded in space [*5*]. All events belong to a single category:

- **pop. III**: **Critical** distribution of spring-block in 2D; ($\gamma_{\Delta,\mathrm{II}} \approx 1.27$):

$$dN(\mathcal{M}_0) \propto \boldsymbol{P}_{\mathrm{III}}(\mathcal{M}_0; s_{\max})dV \; ; \; \boldsymbol{P}_{\mathrm{III}}(\mathcal{M}_0)d\mathcal{M}_0 = \left(\frac{\mathcal{M}_0}{\mathcal{M}_{0,c}}\right)^{-\gamma_{\mathrm{II}}} \frac{\gamma_{\mathrm{II}} - 1}{\mathcal{M}_{0,c}} d\mathcal{M}_0$$

References:
[1] D. W. Eaton, N. Igonin (2020) *The Leading Edge* **37**:2, 135-140
[2] A. McGarr (1976), Journal of *J. of Geophs. Res.* **81**, 1487
[3] C. Dinske, S. Shapiro (2013), *J. Seismol.* **17**: 13: doi:10.1007/s10950-012-9292-9
[4] S. Shapiro, O. Krüger C. Dinske, (2013) *J. of Geophs. Res. Solid Earth* **118**, 3557
[5] N. van der Elst et al. (2016), *J. of Geophs. Res. Solid Earth* **121**, 4575
[6] J. Norris, D. Turcotte, J. Rundle (2014), *Physical Review E* **89**, 022119
[7] Y. Ben-Zion, J. Rice (1993), *J. of Geophs. Res. Solid Earth* **98**, 14109
[8] A. McGarr (2014), *J. of Geophs. Res. Solid Earth* **119**, 1008

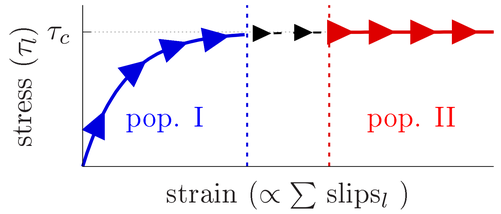

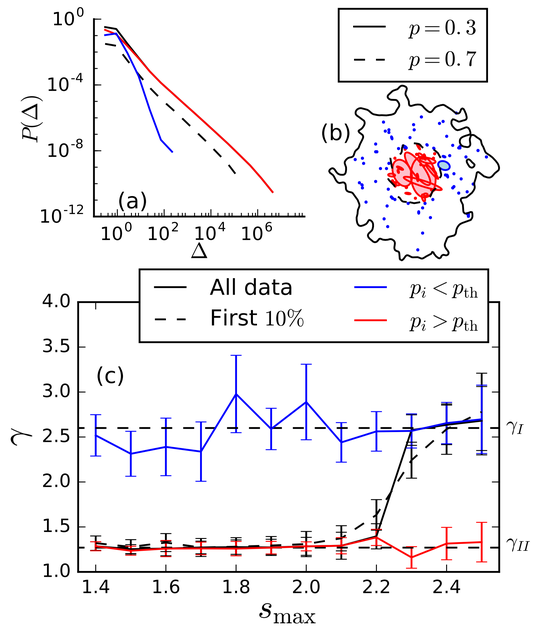

In the case $\mathcal{M}_0 \sim \Delta$. By fitting $\{\hat{\mathbf{x}}_{\mathbf{II}}, \hat{\mathbf{\Lambda}}, \hat{\eta}\}$, $s_{\max} = 2.2$. Cumulative number larger than Δ, as in [*3,4*]:

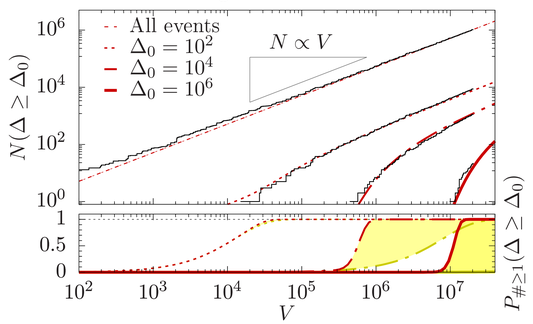

Max. magnitude as function of V as in [*1*]:

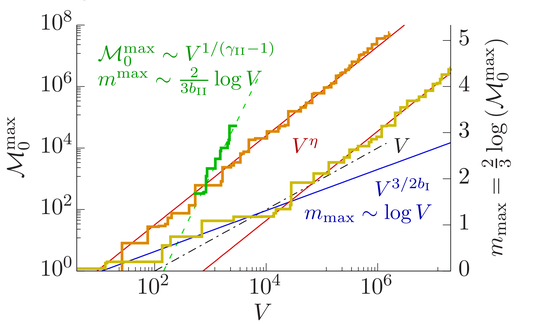

- proportionality: $\mathcal{M}_0^{\max} \sim V$ (exponents in [*8*]).
- **pop. I** dominates (small events, models [*2,3*]).
- **pop. II** dominates (bounded events, model [*4*]).
- **high** stress level ($s_{\max} = 1.4$), always pop. II.
- **low** stress level ($s_{\max} = 2.2$), **pop. I** $\rightarrow$ **pop. II**.
- **Tectonic** setting (**pop III**) (model [*5*]).